Available online at www.sciencedirect.com
ScienceDirect
Journal of Sound and Vibration 311 (2008) 1358–1370
JOURNAL OF SOUND AND VIBRATION
www.elsevier.com/locate/jsvi

Measurement nonlinearity interpreted as material behavior in dynamic nanoindentation

B.P. Mann[a,*], J. Liu[b], S.S. Hazra[c]

[a]Department of Mechanical Engineering and Materials Science, Duke University, Durham, NC 27708, USA
[b]Department of Mechanical and Aerospace Engineering, University of Florida, Gainesville, FL 32611, USA
[c]Department of Mechanical and Aerospace Engineering, University of Missouri-Columbia, Columbia, MO 65211, USA

Received 2 November 2006; received in revised form 26 September 2007; accepted 12 October 2007
Available online 26 November 2007

Abstract

This paper explores the errors that may arise in when interpreting dynamic nanoindentation measurements with a linear oscillator model. The work was motivated by an experimental observation that the system's primary resonance can be dramatically altered by changes in loading conditions. Investigations elucidate that different sources of nonlinearity can interact to alter the identified contact stiffness which will manifest itself as a change in the system's primary and secondary resonances.

The errors associated with interpreting dynamic indentation measurements with a linear model are investigated through modeling, analysis, and numerical study. Theoretical efforts show that measurement nonlinearity can be falsely interpreted as material behavior. Hence, the common practice of applying a linear oscillator model is expected to sometimes lead to significant errors. These finding suggest that a nonlinear analysis may often be required to improve measurement interpretations.

1. Introduction

Studying the nanomechanical response of material surfaces has received much attention in recent years [1–8]. These studies have been motivated by the development of new nanostructured materials, a continued miniaturization within engineering, semiconductor components, thin film technology, and a growing interest in the characterization of soft biomaterials [4,9]. For example, surface characterization is essential for the semiconductor industry since properties like hardness and moduli can have a significant effect on yield, performance, and device longevity [10]. As a second example, consider the *in vivo* performance of biomaterials where an understanding the surface chemistry and biocompatability are essential considerations [11]. Inadequate surface mechanical properties may lead to premature failure due to wear, fracture, and surface fatigue mechanisms. In addition, recent research suggests that cells respond to mechanical stimuli which links the performance of biomedical devices and engineered biomaterials, such as artificial skin and cartilage,

*Corresponding author.
E-mail address: brian.mann@duke.edu (B.P. Mann).

0022-460X/$ - see front matter © 2007 Elsevier Ltd. All rights reserved.
doi:10.1016/j.jsv.2007.10.023

to submicron mechanical behavior [11,12]. Therefore, the need to accurately characterize nanoscale mechanical material behavior is of utmost importance.

Some of the primary instruments developed for surface studies include: (1) the atomic force microscope (AFM); (2) the surface force apparatus (SFA); and (3) a depth-sensing indentation. The capabilities of these instruments cover a wide range of contact area—from several micrometers down to a few nanometers. The SFA is mainly suited for direct measurements of surface and intermolecular forces (i.e. not mechanical material behavior). The AFM is a popular instrument for imaging surface topography which has also been used to investigate the elastic and plastic properties of materials at the nanoscale (e.g. see Refs. [2,10,13]). However, indentation-based AFMs suffer quantitatively due to an unknown contact area of the AFM tip and transducer issues that include piezo-creep, nonlinearity, and hysteresis [8].

The accurate determination of both contact area and displacement have been improved by recent developments in depth-sensing indentation [8,14,15]. The underlying principle is to couple depth sensing with force modulation to obtain more quantitative measures of mechanical material behavior. During a typical nanoindentation process, a load is applied to an indenter and the penetration depth is measured as a function of load. For quasi-static nanoindentation measurements, it is common to use the slope of the unloading portion of the load–displacement curve to extract the material's elastic modulus [14–18]. However, quasi-static test results are often incomplete since no information about the material's energy dissipation characteristics under oscillatory loads is revealed.

To study the surface properties under cyclic loading, it is necessary explore the dynamic response of the combined indenter/material system at the nanometer scale. While previous dynamic nanoindentation studies have provided linear parameter estimation schemes, which rely upon the monitored response amplitude and phase relationships [9,19,20], little is known about the influence of measurement nonlinearities in dynamic nanoindentation. Therefore, the current study was launched to investigate the influence of measurement nonlinearities on the estimated mechanical properties.

The work of this investigation is organized as follows. Since this research was motivated by the experimental observation that the system's primary resonance could be dramatically altered by changes in the static loading, some sample experimental results are presented in the next section. Although the resonance shift is already well known within the nanoindentation community, the authors note that this phenomenon is also affirmation that nonlinear effects may be important. Suspecting the resonance shift to be the result of multiple nonlinear interactions, the current investigation was launched to study the role of nonlinearities in the tip-sample interaction force and in the transducer of a commercially available nanoindentation instrument. The third section presents a model for the nanoindentation process which is later studied numerically and theoretically.

A primary outcome from this investigation is the realization that nonlinearities in the measurement process could be falsely interpreted as material behavior—as in the case of applying a linear oscillator model for interpretation. This assertion is supported by theoretical efforts that explore the errors associated with using a linear oscillator model and the beneficial role of nonlinear analysis in obtaining more quantitative nanomechanical properties.

2. Experimental study and observations

To illustrate the qualitative role of nonlinearity during indentation testing, a series of dynamic nanoindentation experiments were performed on polytetraflourethylene (PTFE) using a commercially available Hysitron Inc. nanoindenter. The primary instrumentation used during the experimental study was a capacitive load–displacement transducer, a lock-in amplifier, and displacement sensing electronics. The indenter load–displacement transducer, shown in Fig. 1, has rigid top and bottom plates that sandwich a rigidized middle plate which is supported by compliant outer springs; these plates are used to position the indenter tip with electrostatic forces that are generated from applied voltages. Displacements of the transducer middle plate are then sensed by monitoring changes in capacitance.

Prior to performing dynamic indentation experiments, a series of calibration tests were performed on the electrostatic transducer—while the indenter tip is out of contact with the material specimen. Transducer

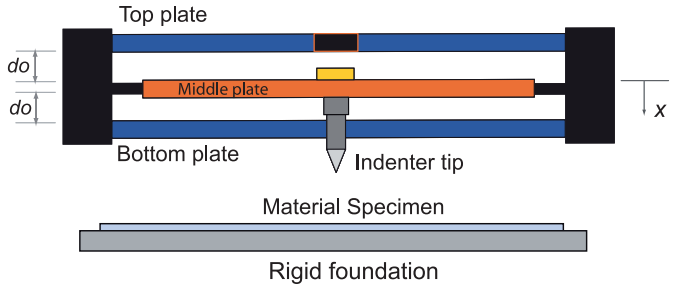

Fig. 1. Nanoindentation transducer schematic for a three-plate electrostatic transducer and material specimen in a typical nanonindentation test.

Table 1
Experimentally identified model parameters that were applied during numerical studies

Parameter	Value	Units
m	260×10^{-6}	kg
c	4.70×10^{-2}	N s/m
k	160	N/m
E	2×10^{8}	N/m^2
R	2×10^{-6}	m
A	53.85×10^{-6}	m^2
d_0	87×10^{-6}	m

calibration was performed by applying a quasi-static ramp voltage between two transducer plates and monitoring the change in the capacitance. To extract the mechanical model terms for the first mode of vibration, frequency sweep tests were performed in air. Table 1 provides the numerical values for the transducer model parameters that are defined in the next section.

All tests were performed with a diamond sphero-conical tip since this tip is particularly suited for measuring soft materials [14]. Since imperfections in the geometric shape of the indenter tip are known to alter the load–displacement curve [18], the profile of the indenter tip was checked with a scanning electron microscope (see image in Fig. 3). Here, the scaled image has been imported into Autocad and fitted with a paraboloid to determine the tip radius of curvature.

A specific goal of the experiments was to elucidate the influence of nonlinearities on the dynamic response of the system. In particular, the curvature of a typical quasi-static load–displacement curve suggests a "spring hardening" effect that occurs for an increased indentation depth. This also suggests that the observed primary resonance could be altered by changes in the static load, dynamic load, or by oscillation amplitude of the transducer. Therefore, a specific aim of the experimental tests was to capture resonance shifts by varying the static transducer load for a constant dynamic load.

Fig. 2 shows two series of dynamic nanoindentation experiments performed at static loads of 300 and 500 μN, but for the same dynamic load of 50 μN. As anticipated, a noticeable shift occurs in the system's primary resonance for the two different static loads. In the sections that follow, we show that the change in the system's resonance is due to measurement nonlinearities that are inherent to the tip–sample interaction force and the electrostatic transducer. While it is common to apply a linear oscillator model and state that the static loading has caused a change in the contact stiffness, we will highlight some effects that are overlooked by this common practice.

The material properties of a material surface are often estimated from the response amplitude and phase relationships during dynamic nanoindentation. The typical approach is to apply a linear oscillator model to determine a linear contact stiffness and subsequently determine the material properties from a contact model

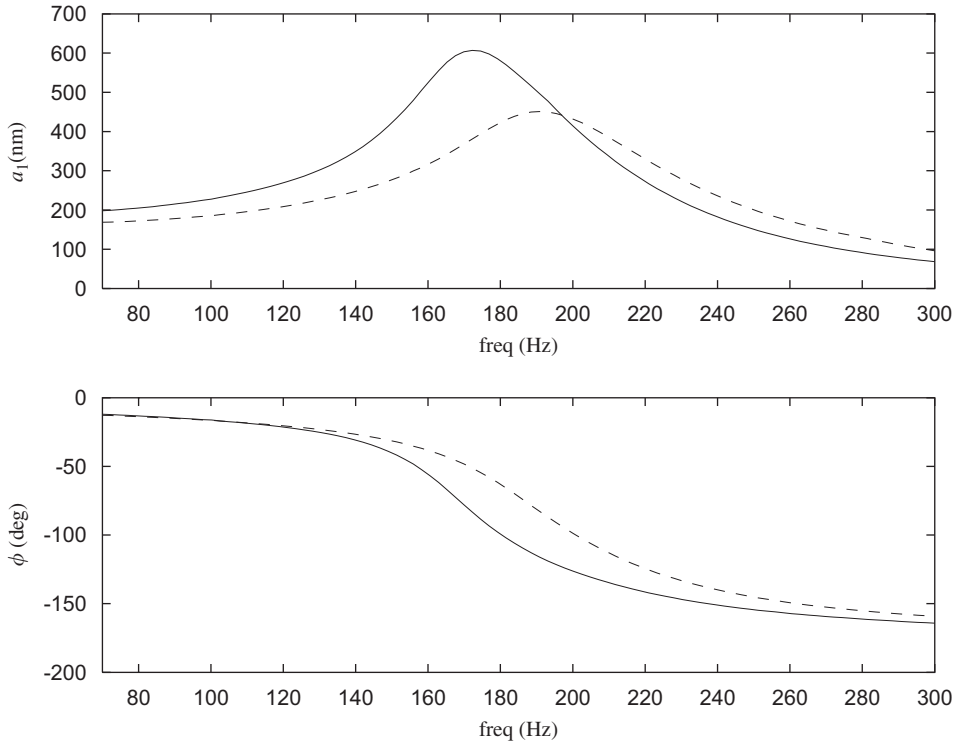

Fig. 2. Experimental dynamic nanoindentation test data showing the response amplitude and phase results at the excitation frequency for two different static loads. A solid line indicates a 300 μN static load and a dashed line represents a 500 μN static load.

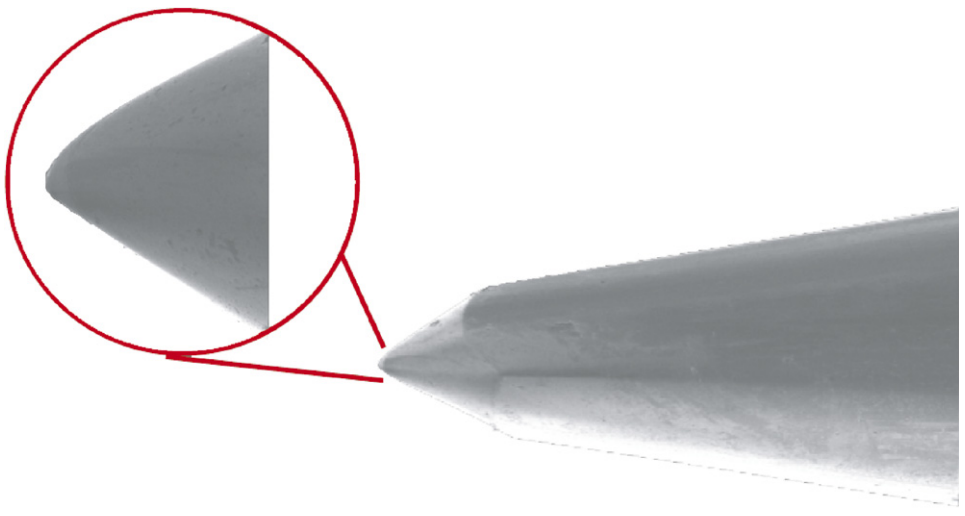

Fig. 3. Scanning electron microscope image of the nanoindenter tip. This image was used to better approximate the conospherical indenter tip radius which was determined to be $R \approx 2\,\mu m$.

(e.g. see example contact models in Refs. [21–24]). Thus, this paper investigates two theoretical scenarios: (1) the errors that occur when applying a linear oscillation model to a indenter system when the contact model is Hertzian and (2) the role of nonlinear analysis in correcting the errors that occur from the choice of using a linear analysis (Fig. 3).

3. Nanoindentation model

This section develops a model for the capacitive transducer used in the previously shown experimental tests. The indenter transducer is assumed to have a rigidized middle plate that is held with compliant supporting springs, a perforated rigid top plate, and a perforated rigid bottom plate (see Fig. 1). Using the parallel-plate assumption, the capacitances of the top and bottom capacitors can be written as

$$C_T(x) = \frac{\varepsilon_r \varepsilon_0 A}{x + d_0} \quad \text{and} \quad C_B(x) = \frac{\varepsilon_r \varepsilon_0 A}{d_0 - x}, \tag{1}$$

where A is the capacitor plate area, $\varepsilon_0 = 8.854 \times 10^{-12}\,\mathrm{C}^2/(\mathrm{N\,m}^2)$ is the permittivity constant of a vacuum [25], $\varepsilon_r = 1.005$ is the relative permittivity constant of air [25], x is the displacement of the middle plate, and d_0 is the initial gap spacing between the plates at the zero volt equilibrium position.

The resulting potential energy, $U(x)$, for the first mode of the discretized system is

$$U(x) = \frac{k}{2}x^2 + \frac{1}{2}C_T(x)V_T^2 + \frac{1}{2}C_B(x)V_B^2, \tag{2}$$

where k is the first modal stiffness and V_T and V_B are the voltages applied to the top and bottom plates of the transducer, respectively. After using Lagrange's equation, the equation of motion for the middle plate is found to be

$$m\ddot{x} + c\dot{x} + kx + F_{\mathrm{TS}}(x, \dot{x}) = \frac{\varepsilon_r \varepsilon_0 A}{2}\left[\frac{V_B^2}{(d_0 - x)^2} - \frac{V_T^2}{(x + d_0)^2}\right], \tag{3}$$

where m is the first modal mass, c is a viscous damping coefficient, and $F_{\mathrm{TS}}(x, \dot{x})$ is the tip–sample interaction force during contact.

During a typical dynamic nanoindentation test, the voltage on the top plate is typically set to zero and a voltage is applied to the middle and bottom plates. The voltage potential on the transducer middle and bottom plates is comprised of a constant and a single harmonic component $V_B = V_{\mathrm{DC}} + V_{\mathrm{AC}}\cos\Omega t$. Therefore, the resulting input to the system contains both a constant and multiple harmonic terms—given by the square of the input voltage

$$V_B^2 = \left(V_{\mathrm{DC}}^2 + \frac{V_{\mathrm{AC}}^2}{2}\right) + 2V_{\mathrm{DC}}V_{\mathrm{AC}}\cos\Omega t + \frac{V_{\mathrm{AC}}^2}{2}\cos 2\Omega t. \tag{4}$$

To further generalize the presented results, Eq. (3) is nondimensionalized by the introduction of a nondimensional time, $\tau = \omega t$ where $\omega = \sqrt{k/m}$ is the mechanical resonance, and a nondimensional displacement $y = x/d_0$. The resulting equation is

$$y'' + 2\zeta y' + y + F_{\mathrm{TS}}(y, y') = \frac{1}{(1 - y)^2}[F_0 + F_1\cos\eta\tau + F_2\cos 2\eta\tau], \tag{5}$$

where $2\zeta = c/(m\omega)$ is a damping term and $\eta = \Omega/\omega$ represents the ratio of the excitation frequency to the transducer's natural frequency. The remaining terms on the right-hand side of Eq. (5) are $F_0 = \beta(V_{\mathrm{DC}}^2 + V_{\mathrm{AC}}^2/2)$, $F_1 = 2\beta V_{\mathrm{DC}}V_{\mathrm{AC}}$, $F_2 = \beta V_{\mathrm{AC}}^2/2$, and $\beta = \varepsilon_r\varepsilon_0 A/(2md_0^3\omega^2)$.

4. Methods for error correction

This section investigates the errors associated with interpreting dynamic nanoindentation data with a linear oscillator model and provides an alternative for error correction. For the sake of simplicity, the tip–sample interaction force is assumed to be dominated by the elastic conformal contact of a spherical tip and a flat material surface. Empirical data is generated from numerical simulation to demonstrate that the simplified tip–sample interaction force model qualitatively captures the resonance shifts observed during experimental study. The errors associated with imposing a linear oscillator model are then examined. Since it is unveiled that substantial errors will sometimes occur, methods for error correction are discussed.

The numerical and theoretical results that follow assume a nondimensionalized version of a Hertzian contact force,

$$F_{\mathrm{TS}}(y,y') = \frac{4}{3k}\sqrt{Rd_0}Ey^{3/2}, \tag{6}$$

where E is the reduced modulus and R is the radius of the indenter. Although this model does not include the influence of adhesive or viscoelastic forces, it does serve as a representative contact model for elastic materials with little surface energy.

Numerical studies of Eq. (5) were used to investigate the qualitative trends in the system's primary resonance. In particular, our goal was to show that the theoretical model qualitatively captures the same resonance shift. Thus the model parameters used for the numerical studies, with the exception of the reduced modulus, were the actual parameters obtained from the initial calibration tests performed on the electrostatic transducer (see Table 1). In an effort mimic the previously shown experimental tests, where the dynamic load was held constant, F_1 was held to a constant value during simulation and the values of F_0 and F_2 were altered for each of the three cases investigated.

Fig. 4 compares the spectral amplitudes of the primary response and the first harmonic (the 2η response) for three loading conditions against a reference case—where the reference case used the following values ($F_0 = 3.63 \times 10^{-3}$ and $F_2 = 3.99 \times 10^{-6}$). The spectral response amplitudes, which primarily consisted of a constant response a_0, a response at the excitation frequency a_1, and a response at the first super harmonic a_2, were extracted from the numerically generated time series. As observed in the experimental tests, a noticeable

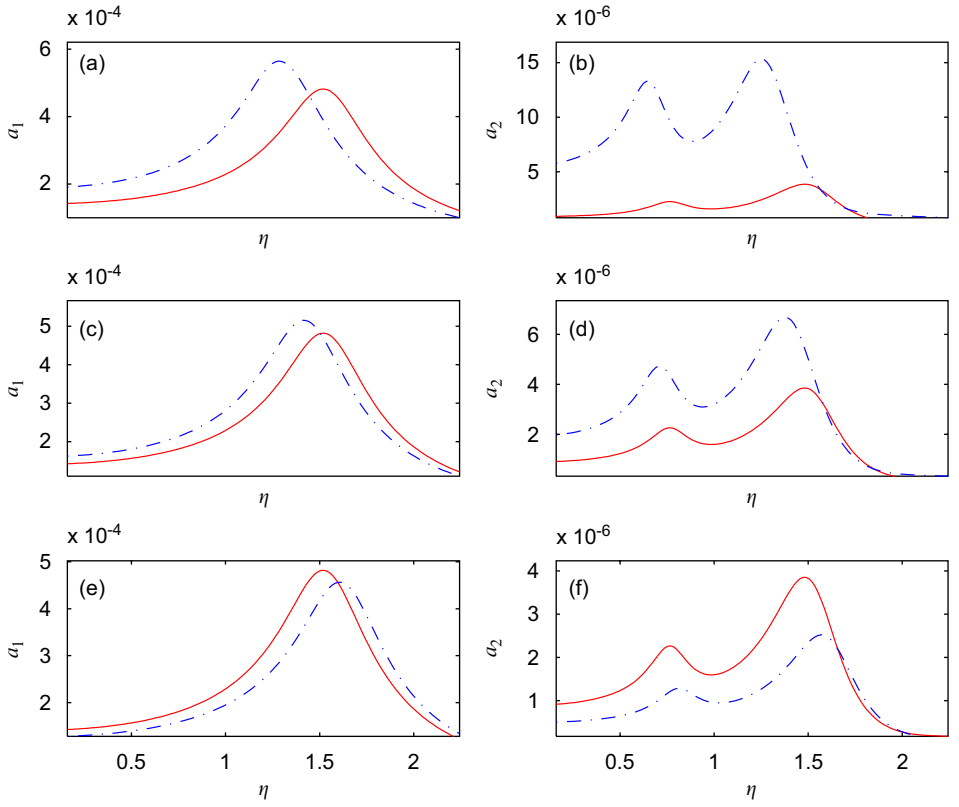

Fig. 4. Spectral amplitude curves generated from numerical simulation of Eq. (5) for a constant $F_1 = 3.40 \times 10^{-4}$ value. Left column is the response at the excitation frequency and the right column is the response at twice the excitation frequency. Graphs compares spectral amplitudes with a reference case (solid red line) that was generated using $F_0 = 3.63 \times 10^{-3}$ and $F_2 = 3.99 \times 10^{-6}$. The reference case acts as a baseline when comparing the resonant peaks of the other loading conditions. The following parameters were used for the dotted blue line results: for graphs (a) and (b) $F_0 = 9.22 \times 10^{-4}$ and $F_2 = 1.60 \times 10^{-5}$; for graphs (c) and (d) $F_0 = 2.04 \times 10^{-3}$ and $F_2 = 7.09 \times 10^{-6}$; for graphs (e) and (f) $F_0 = 5.66 \times 10^{-3}$ and $F_2 = 2.55 \times 10^{-6}$.

shift in system's primary resonance is evident for the numerical data. However, these graphs additionally reveal a shift in the system's secondary resonance. Since the most critical question is how these trends affect surface characterization results, the next section investigates the errors associated with the commonly applied linear oscillator model.

4.1. Local linearization approach

This section investigates the errors associated with applying a linear oscillator model and an approach for improving surface characterization results by tracking the shift in the system's primary resonance. More specifically, it is common to measure the response amplitude and phase relationships during dynamic indentation. These measurements are then interpreted with a linear oscillator model to determine the contact stiffness and/or the nanomechanical properties. The presented results apply a linear oscillation model by linearizing the system about the static indentation depth δ_0—where the static indentation depth is the equilibrium position when V_{AC} is set to zero in the expressions for F_0, F_1, and F_2. In essence, the presented approach is equivalent to studying the linear oscillations about the nonlinear equilibrium position.

The assumed form for the linear oscillator model is

$$y'' + 2\zeta y' + \omega_0^2 y = F_D \cos \eta\tau, \tag{7}$$

where ω_0 is a local linear resonance value and F_D is a local dynamic excitation term which will later be related to F_1 in Eq. (5). Since the localized equation is assumed to be linear, the terms F_0 and F_2, which appear in Eq. (5), can be disregarded based on the principle of superposition. The response amplitude and phase relationships for Eq. (7) are

$$a_1 = \frac{F_D}{\sqrt{(\omega_0^2 - \eta^2)^2 + (2\zeta\eta)^2}}, \tag{8a}$$

$$\phi = \tan^{-1}\left(\frac{-2\zeta\eta}{\omega_0^2 - \eta^2}\right). \tag{8b}$$

To better understand the errors of applying a linear oscillator model, numerical studies were performed in Eq. (5) using $F_0 = 1.42 \times 10^{-3}$, $F_1 = 3.39 \times 10^{-4}$, and $F_2 = 1.02 \times 10^{-5}$. The resulting spectral amplitudes, shown in Fig. 5, are presented along with the resulting errors in the identified modulus. For instance, larger errors in the estimated reduced modulus are shown to occur for relatively larger oscillations near the system's primary resonance—where the term $\%|\Delta E/E|$ is the percent difference between the estimated reduced modulus and the actual reduced modulus given in Table 1.

A second case, shown in the results of Fig. 6, was investigated for the parameters $F_0 = 6.92 \times 10^{-3}$, $F_1 = 1.99 \times 10^{-3}$, and $F_2 = 7.24 \times 10^{-5}$. As in the previous graph, this example shows a trend of increasing errors as the oscillation amplitude increases. However, the error in the estimated modulus is shown to be more than twice the amount of the previous case.

The presented approach is equivalent to identifying a local contact stiffness for parameter identification. To achieve these results, an expression for the local resonance value, ω_0, was obtained by expanding the nonlinear relationships for the tip–sample and electrostatic forces about the transducer mean position. The influence of the electrostatic term is approximated from the first term on the right-hand side of Eq. (5) (i.e. $F_e = F_0/(1-y)^2$). This term is expanded about the transducer mean position, $y = a_0$, to obtain

$$F_e \approx \frac{F_0}{(1-\delta_0)^2} + \frac{2F_0}{(1-\delta_0)^3}(y - \delta_0), \tag{9}$$

where terms on the order of $\mathcal{O}(y^2)$ and higher have been neglected. Similarly, expanding the tip–sample contact force about the transducer mean position results in

$$F_{TS}(y, y') \approx \frac{4E\sqrt{Rd_0}\delta_0^{3/2}}{3k} + \frac{2E\sqrt{Rd_0\delta_0}}{k}(y - \delta_0). \tag{10}$$

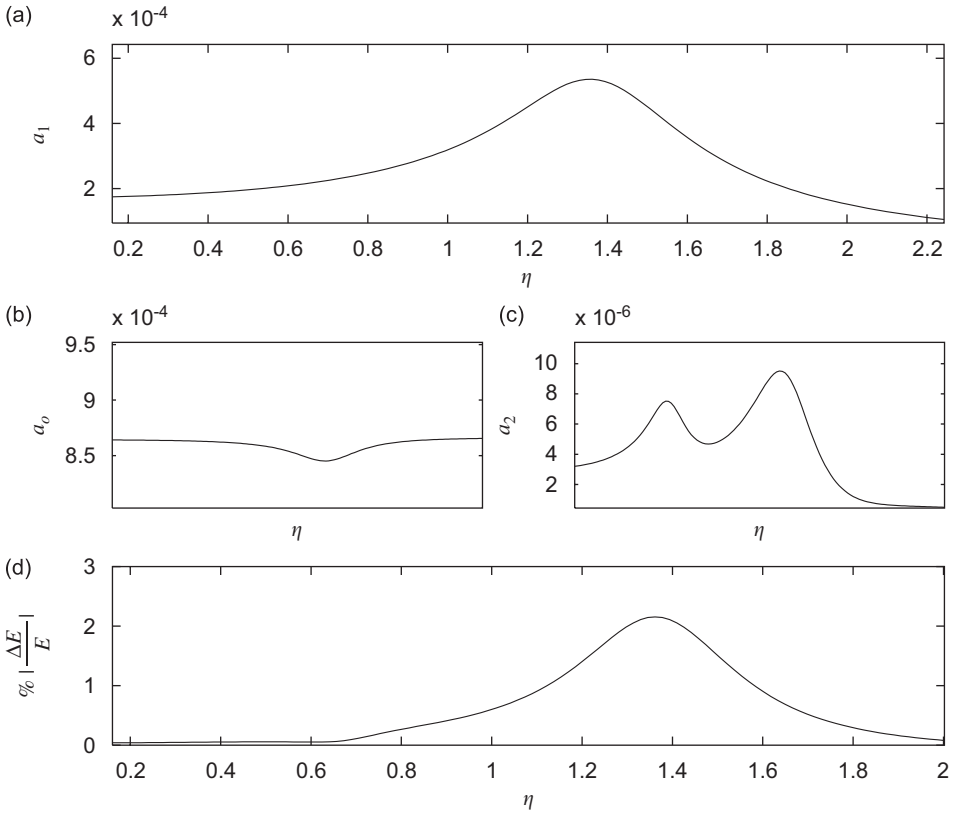

Fig. 5. Numerically predicted spectral amplitude responses are shown in graphs (a–c) for $F_0 = 1.42 \times 10^{-3}$, $F_1 = 3.39 \times 10^{-4}$, and $F_2 = 1.02 \times 10^{-5}$. The legend for each plot is as follows: (a) the response at the excitation frequency, (b) the mean response, (c) the response at twice the excitation frequency, and (d) the errors of applying a linear oscillator model with corrections for both the electrostatic and tip–sample nonlinearities.

An expression for the local resonance is found by collecting the coefficients of y in Eqs. (8) and (10) to obtain

$$\omega_0^2 \approx 1 + \frac{2E\sqrt{Rd_0\delta_0}}{k} - \frac{2F_0}{(1-\delta_0)^3}. \tag{11}$$

The final correction for the electrostatic nonlinearity requires relating F_D to F_1 by localizing the first dynamic excitation term about the transducer mean position

$$F_D = \frac{F_1}{(1-\delta_0)^2}. \tag{12}$$

In summary, the results of this section use gradient relationships for the nonlinear forces to obtain localized values. This approach is equivalent to the common process of identifying a local contact stiffness. While implementing a local resonance from linearization does greatly reduce the errors in the estimated system parameters, this approach is somewhat limited since the corrections are localized values. In particular, this section provides evidence to suggest that the quantification errors will increase with the oscillation amplitude. These results elucidate a specific limitation of a linear oscillator model—the inability to capture the nonlinear contact stiffness terms. For the presented results, this is validated by the fact that errors sharply increase as the system's primary resonance is approached (see Figs. 5 and 6). Thus, it makes sense to consider alternative strategies that can mitigate the errors associated with a linear oscillator model. One approach to alleviate the aforementioned errors is to apply a nonlinear analysis. The next section describes a nonlinear analysis which can be implemented for improved parameter identification.

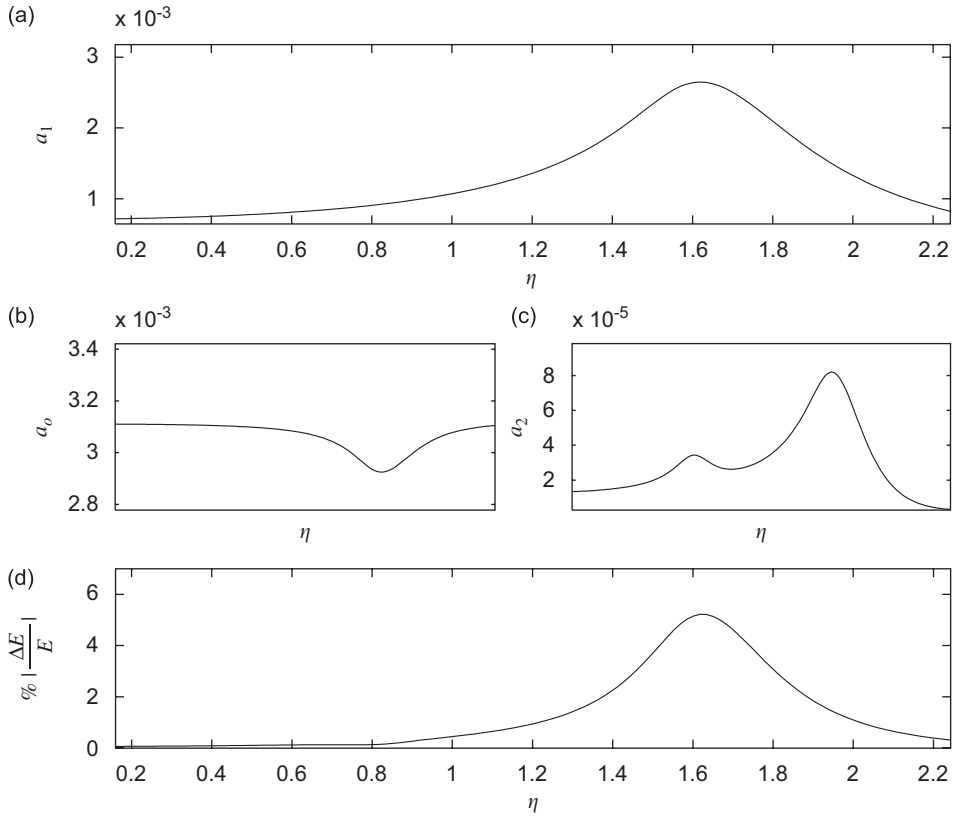

Fig. 6. Numerically predicted spectral amplitude responses, graphs (a and c), for $F_0 = 6.92 \times 10^{-3}$, $F_1 = 1.99 \times 10^{-3}$, and $F_2 = 7.24 \times 10^{-5}$. The legend for each plot is as follows: (a) the response at the excitation frequency, (b) the mean response, (c) the response at twice the excitation frequency, and (d) the errors of applying a linear oscillator model with corrections for both the electrostatic and tip–sample nonlinearities.

4.2. Comparisons to nonlinear identification

This section describes a nonlinear identification approach that can be used to obtain more quantitative results for the contact forces and/or material properties. Errors from the nonlinear identification approach are then compared with the errors of the local linearization. In the Harmonic Balance nonlinear identification approach, the steady-state response of the system is written as a truncated Fourier series whose fundamental frequency is related to the excitation frequencies [26]. For example, the response of the system is written as the following Fourier expansion:

$$y(t) = \sum_{p=0}^{N} a_p \frac{e^{ip(\eta t+\phi)} + e^{-ip(\eta t+\phi)}}{2}, \tag{13}$$

where N describes the number of terms in the expansion and ϕ is the phase shift between the excitation signal and the output response. To help obtain an approximate analytic solution, a parametric expression is assumed for the tip–sample interaction force,

$$F_{TS}(y, y') = 2\mu y' + \alpha_0 + \alpha_1 y + \alpha_2 y^2 + \alpha_3 y^3, \tag{14}$$

which has coefficients to capture the viscoelastic and nonlinear restoration forces. If it is assumed that $N = 2$ for Eq. (13), both Eqs. (13) and (14) can be substituted into Eq. (5) and the terms of the same harmonics can be equated into real and imaginary components. The result is a set of equations that relate the excitation harmonics to the spectral amplitudes and relative phase response of the system. While these relationships are

nonlinear functions of the response amplitude and phase relationships, they are linearly related to the unknown parameters of the differential equation. Eq. (15) is a matrix equation that relates the unknown parameters of the system to the measured spectral amplitudes

$$\begin{bmatrix} B_{11} & B_{12} & B_{13} & B_{14} & B_{15} \\ B_{21} & B_{22} & B_{23} & B_{24} & B_{25} \\ B_{31} & B_{32} & B_{33} & B_{34} & B_{35} \\ B_{41} & B_{42} & B_{43} & B_{44} & B_{45} \\ B_{51} & B_{52} & B_{53} & B_{54} & B_{55} \end{bmatrix} \begin{bmatrix} \mu+\zeta \\ \alpha_0 \\ 1+\alpha_1 \\ \alpha_2 \\ \alpha_3 \end{bmatrix} = \begin{bmatrix} D_1 \\ D_2 \\ D_3 \\ D_4 \\ D_5 \end{bmatrix}, \tag{15}$$

which may be rewritten in a more compact form as $\mathbf{BC} = \mathbf{D}$. The unknown system parameters can then be found by simply multiplying both sides of Eq. (15) by the inverse of $\mathbf{B}$. This approach was investigated for both $N = 2$, as shown in Eq. (15), and for $N = 1$ with nearly negligible differences in the identified modulus. However, using $N = 1$ reduces the number of equations to three, or three rows for the $\mathbf{B}$-matrix of Eq. (15), which requires an additional measurement to be taken at a neighboring frequency to make the number or rows greater than the number of unknowns. In an effort to minimize the presented complexity, the lengthy expressions that populate Eq. (15) for $N = 1$ have been listed in the appendix—see Eqs. (A.1)–(A.3).

The procedure for identifying the reduced modulus of Eq. (6) required relating α_0–α_3 of Eq. (14) to the Taylor series expansion of Eq. (6) about the mean transducer position. The coefficients used to relate the contact force to the reduced modulus were

$$\alpha_0 = -\frac{E\sqrt{Rd_0}a_0^{3/2}}{12k}, \tag{16a}$$

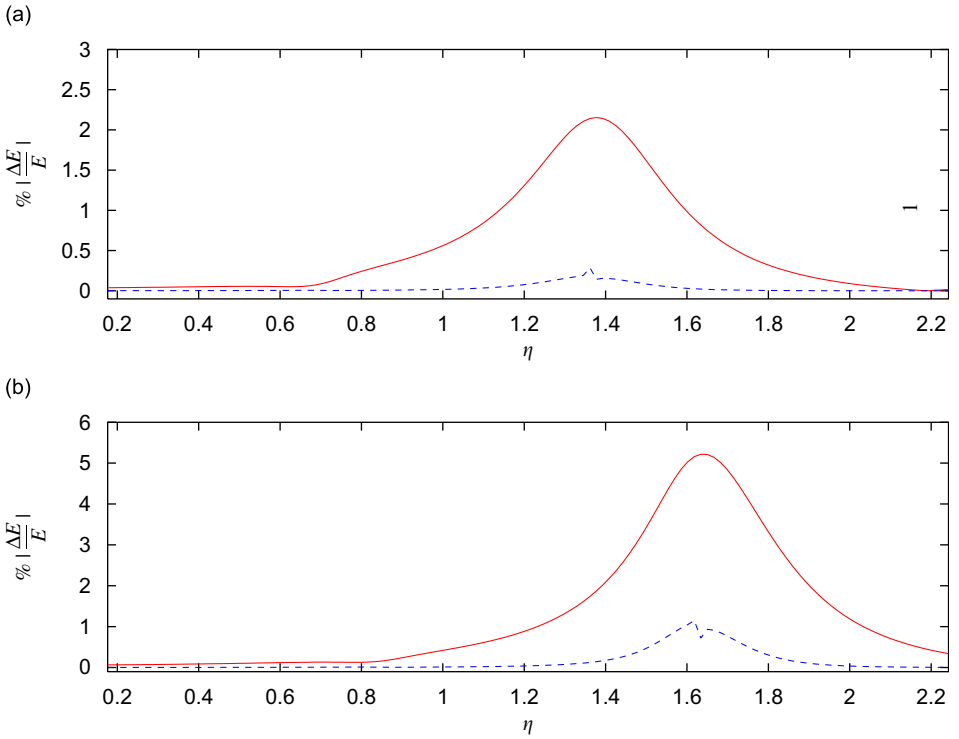

Fig. 7. Errors from local linearization (solid red line) are compared to the harmonic balance nonlinear identification approach (dotted blue line). Presented results are for the same parameters as (a) corresponds to the results of Fig. 5 and (b) corresponds to the results of Fig. 6.

$$\alpha_1 = \frac{3E\sqrt{Rd_0a_0}}{4k}, \tag{16b}$$

$$\alpha_2 = \frac{3E\sqrt{Rd_0}}{4k\sqrt{a_0}}, \tag{16c}$$

$$\alpha_3 = -\frac{E\sqrt{Rd_0}}{12ka_0^{3/2}}. \tag{16d}$$

Since multiple realizations of the reduced modulus can be obtained from the coefficients α_0–α_3, the least-square error of $F_{TS}(y, y')$ over the range of a_1 was used. Fig. 7 compares the errors from the nonlinear identification approach to those of the local linearization method. The presented cases are the same as those studied in Figs. 5 and 6. In both these figures, and in the numerous other cases investigated, the nonlinear identification approach greatly reduces the errors in the identified modulus.

5. Conclusions

Indentation testing has become a popular method for surface characterization. This paper states that measurement nonlinearities are responsible for the observed changes in the estimated contact stiffness and material properties that occur under different loading conditions. The justification proceeds begins by presenting phenomenological data from experimental dynamic nanoindentation tests that show a qualitative change in system's primary resonance. Although a resonance shift is common knowledge to some researchers, the fact that errors may arise when interpreting dynamic tests with a linear oscillator model has not received any attention. This fact has motivated the authors to examine the errors that may arise when using a linear oscillator model to interpret dynamic nanoindentation tests.

After presenting experimental evidence that illustrates a phenomenological trend in the system's primary resonance, the manuscript then explores the notion that nonlinearity in the measurement process could sometimes skew measurement interpretations. In particular, if a linear oscillator models is applied for measurement interpretation, we show measurement nonlinearities can be falsely interpreted as material behavior. This suggests that system nonlinearities should be included in modeling efforts aimed at quantitative characterization of material surfaces with indentation testing. Furthermore, nonlinear identification schemes should also be implemented to obtain the most accurate results.

In an effort to provide conclusive evidence of our hypothesis, we have chosen to perform numerical and theoretical studies that mimic the experimental situation. Modeling efforts apply a Hertzian contact model to describe the tip–sample interaction force and develop a model for the commercially available nanoindentation transducer. After demonstrating that the numerical studies show qualitative agreement with the experimentally observed resonance shift, we investigate our assertion that measurement nonlinearities can be falsely interpreted as material behavior through the application of a linear parameter estimation technique. Furthermore, error corrections are investigated by applying linearization about the nonlinear equilibrium position before presenting the results of a more comprehensive nonlinear analysis.

In summary, the experimentally observed primary resonance shift phenomenon motivated us to investigate whether nonlinearity could cause errors in the identification of the nanomechanical properties with a linear oscillator model. Numerical studies are used to confirm that measurement nonlinearities will interact to alter the system's primary and secondary resonances which will also skew the results of applying a linear identification scheme. Finally, it is shown that unwanted errors in the identification process can be minimized through the implementation of a nonlinear identification procedure.

While the authors believe the present work confirms our hypothesis that measurement nonlinearities can be falsely interpreted as material behavior, we acknowledge that present study does not investigate an upper bound. Thus, we believe one area of future investigation would be to determine the parameter space regions where the errors are the most and least prevalent. Along this direction, we have observed in preliminary work that the nonlinear terms become more influential as the static indentation depth is decreased and oscillation

amplitude is increased. Thus, we expect linear analysis errors to be more substantial for dynamic nanoindentation than they would be for microindentation.

Acknowledgements

The authors would like to thank S. Asif and O. Warren of Hysitron, Inc. for discussing the results of this paper. Research support from US National Science Foundation Award (CMII- 0556150) is also gratefully acknowledged.

Appendix A. Harmonic Balance matrix terms

The first row of Eq. (15) are the constants that are equated from the Harmonic Balance approach. These terms are given by

$$\begin{aligned}
B_{11} &= 0,\\
B_{12} &= (1-a_0)^2 + \tfrac{1}{2}a_1^2,\\
B_{13} &= a_0(1-a_0)^2 + a_1^2(\tfrac{3}{2}a_0 - 1),\\
B_{14} &= a_1^2(\tfrac{3}{8}a_1^2 + \tfrac{1}{2} + 3a_0(a_0-1)) + a_0^2(1-a_0)^2,\\
B_{15} &= a_1^4(\tfrac{15}{8}a_0 - \tfrac{3}{4}) + a_1^2 a_0(5a_0^2 - 6a_0 + \tfrac{3}{2}) + a_0^3(a_0-1)^2,\\
D_1 &= F_0 - a_1^2\eta^2(1-a_0).
\end{aligned} \tag{A.1}$$

The second row of Eq. (15) includes the real terms from balancing the first harmonic. These terms are

$$\begin{aligned}
B_{21} &= -a_1\eta[(a_0-1)^2 + \tfrac{1}{4}a_1^2]\sin\phi,\\
B_{22} &= a_1(a_0-1)\cos\phi,\\
B_{23} &= a_1[a_0(\tfrac{3}{2}a_0 - 2) + \tfrac{3}{8}a_1^2 + \tfrac{1}{2}]\cos\phi,\\
B_{24} &= a_1(2a_0-1)[a_0(a_0-1) + \tfrac{3}{4}a_1^2]\cos\phi,\\
B_{25} &= a_1[\tfrac{5}{16}a_1^4 + a_1^2(\tfrac{15}{4}a_0^2 - 3a_0 + \tfrac{3}{8}) + a_0^2(\tfrac{5}{2}a_0^2 - 4a_0 + \tfrac{3}{2})]\cos\phi,\\
D_2 &= \frac{F_1}{2} + \frac{1}{8}a_1\eta^2[3a_1^2 + 4(a_0-1)^2]\cos\phi.
\end{aligned} \tag{A.2}$$

The terms of Eq. (15) that comprise the third row are the imaginary terms from balancing that result from balancing the first harmonic. These terms are

$$\begin{aligned}
B_{31} &= a_1\eta[(a_0-1)^2 + \tfrac{1}{4}a_1^2]\cos\phi,\\
B_{32} &= a_1(a_0-1)\sin\phi,\\
B_{33} &= a_1[a_0(\tfrac{3}{2}a_0 - 2) + \tfrac{3}{8}a_1^2 + \tfrac{1}{2}]\sin\phi,\\
B_{34} &= a_1(2a_0-1)[a_0(a_0-1) + \tfrac{3}{4}a_1^2]\sin\phi,\\
B_{35} &= a_1[\tfrac{5}{16}a_1^4 + a_1^2(\tfrac{15}{4}a_0^2 - 3a_0 + \tfrac{3}{8}) + a_0^2(\tfrac{5}{2}a_0^2 - 4a_0 + \tfrac{3}{2})]\sin\phi,\\
D_3 &= \tfrac{1}{8}a_1\eta^2[3a_1^2 + 4(a_0-1)^2]\sin\phi.
\end{aligned} \tag{A.3}$$

References

[1] B. Borovsky, J. Krim, S.A. Asif, K.J. Wahl, Measuring nanomechanical properties of a dynamic contact using an indenter probe and quartz crystal microbalance, *Journal of Applied Physics* 90 (12) (2001) 6391–6396.

[2] S.I. Lee, S.W. Howell, A. Raman, R. Reifenberger, Nonlinear dynamic perspectives on dynamic force microscopy, *Ultramicroscopy* 97 (2003) 185–198.

[3] H.T. Bach, F.J. Steinkruger, W.S. Chamberlin, C.R. Walthers, Quantitative analysis of deuterium and tritium in erbium hydride films of neutron tube targets, *Journal of Vacuum Science and Technology B* 22 (4) (2004) 1738–1745.
[4] J.L. Cuy, A.B. Mann, K.J. Livi, M.F. Teadford, T.P. Weihs, Nanoindentation mapping of the mechanical properties of human molar tooth enamel, *Archives of Oral Biology* 47 (2002) 281–291.
[5] J.Y. Rho, P. Zioupos, J.D. Currey, G.M. Pharr, Variations in the individual thick lamellar properties within osteons by nanoindentation, *Bone* 25 (3) (1999) 295–300.
[6] W.W. Gerberich, N.I. Tymaik, A.A. Volinsky, D.F. Bahr, M.D. Kriese, Nanoindentation-induced defect-interface interactions: phenomena, methods and limitations, *Acta Materialia* 47 (15–16) (1999) 4115–4123.
[7] J.H. Kinney, G.W. Marshall, S.J. Marshall, A micromechanics model of the elastic properties of human dentine, *Archives of Oral Biology* 44 (10) (1999) 813–822.
[8] R.J. Colton, Nanoscale measurements and manipulation, *Journal of Vacuum Science and Technology B* 22 (4) (2004) 1609–1635.
[9] S. Asif, K.J. Walh, R.J. Colten, Nanoindentation and contact stiffness measurements using force modulation with a capacitive load–displacement transducer, *Review of Scientific Instruments* 70 (5) (1999) 2408–2413.
[10] C. Fretigny, C. Basire, Determination of complex modulus by atomic force microscopy, *Journal of Applied Physics* 82 (1) (1997) 43–48.
[11] C. Klapperich, K. Komvopulos, L. Pruit, Nanomechanical properties of polymers determined from nanoindentation experiments, *Journal of Tribology* 123 (1) (2001) 624–631.
[12] C.S. Chen, M. Mrksich, S. Huang, G.M. Whitesides, D.E. Ingberger, Geometric control of cell life and death, *Science* 276 (1997) 1425–1428.
[13] S. Hu, S. Howell, A. Raman, R. Reifenberger, M. Franchek, Frequency domain identification of tip-sample van der waals interactions in resonant atomic force microcantilevers, *Journal of Vibration and Acoustics* 126 (2004) 343–351.
[14] A.C. Fisher-Cripps, Nanoindentation, Mechanical Engineering Series, Springer, New York, 2002.
[15] S. Asif, K.J. Walh, R.J. Colten, O.L. Warren, Quantitative imaging of nanoscale mechanical properties using hybrid nanoindentation and force modulation, *Journal of Applied Physics* 90 (3) (2001) 1192–1200.
[16] X. Chen, J.J. Vlassak, Numerical study on the measurement of thin film mechanical properties by means of nanoindentation, *Journal of Materials Research* 16 (2001) 2974–2982.
[17] E.R. Weppelmann, J.S. Field, M.V. Swain, Observation, analysis, and simulation of the hysteresis of silicon using ultra-micro-indentation with spherical indenters, *Journal of Materials Research* 8 (1993) 830–840.
[18] F.M. Borodich, L.M. Keer, C.S. Korach, Analytical study of fundamental nanoindentation test relationships for indenters of non-ideal shapes, *Nanotechnology* 14 (2003) 803–808.
[19] S. Asif, K.J. Walh, R.J. Colten, The influence of oxide and adsorbates on the nanomechanical response of silicon surfaces, *Journal of Materials Research* 15 (2) (2000) 546–553.
[20] N.A. Burnham, S.P. Baker, H.M. Pollock, Model for mechanical properties nanoprobes, *Journal Material Rsearch* 15 (2000) 2006–2014.
[21] K.L. Johnson, K. Kendall, A.D. Roberts, Surface energy and the contact of elastic solids, *Proceedings of the Royal Society of London A* 324 (1971) 301–313.
[22] B.V. Derjaguin, V.M. Muller, Y.P. Toporov, Effect of contact deformations on the adhesion of particles, *Journal of Colloid an Interface Science* 53 (1975) 314–325.
[23] U.D. Schwarz, A generalized analytical model for the elastic deformation of an adhesive contact between a sphere and a flat surface, *Journal of Colloid an Interface Science* 261 (2003) 99–106.
[24] H. Hertz, On the contact of rigid elastic solids and on hardness, *Verhandlungen des Vereins zur Beförderung des Gerwerbefleisses* 131 (1882) 178–199.
[25] D. Haliday, R. Resnick, *Fundamentals of Physics*, third ed., Wiley, New York, NY, 1988.
[26] K. Yashuda, S. Kawamura, K. Watanabe, Identification of nonlinear multi-degree-of-freedom systems (presentation of an identification technique), *JMSE International Journal* 31 (1988) 8–14.